HHS Public Access

Author manuscript

Neurobiol Aging. Author manuscript; available in PMC 2017 February 02.

Published in final edited form as:

Neurobiol Aging. 2015 January ; 36(1): 505–518. doi:10.1016/j.neurobiolaging.2014.07.011.

Behavioral, neurochemical, and pathological alterations in BAC transgenic G2019S LRRK2 rats

Jang-Won Lee[1,*], **Victor Tapias**[2,*], **Roberto Di Maio**[2], **J. Timothy Greenamyre**[2], and **Jason R. Cannon**[1,#]

[1]School of Health Sciences, Purdue University, 550 Stadium Mall Dr., West Lafayette, IN 47907, USA

[2]Pittsburgh Institute for Neurodegenerative Diseases, University of Pittsburgh, 3501 Fifth Avenue, Pittsburgh, PA, 15260, USA

Abstract

Mutations in leucine-rich repeated kinase 2 (LRRK2) cause autosomal dominant late-onset Parkinson's disease (PD), and the G2019S mutation in the kinase domain of LRRK2 is the most common genetic cause of familial PD. Enhanced kinase activity of G2019S LRRK2 is a suspected mechanism for carriers to develop PD, but pathophysiological function of G2019S LRRK2 is not clear. The objective of the current study was to characterize a bacterial artificial chromosome (BAC) rat expressing human G2019S LRRK2. Immunoblotting analysis showed that G2019S LRRK2 expression was ~5–8 times higher than wild-type (WT) rat LRRK2. At ages of 4, 8, and 12 months, our characterization showed that expression of G2019S LRRK2 induced oxidative stress in striatum and substantia nigra, increased inducible nitric oxide synthase expression in nigral dopamine neurons, and abnormal morphology of nigral dopaminergic neurons in TG rats compared to WT, without inducing overt neurodegeneration in nigrostriatal dopaminergic neurons. Thus, we conclude that while this model does not reproduce the key features of end-stage PD, important preclinical features of the disease are evident, which may be useful in studying the earliest stages of PD and for gene-environment interaction studies.

Keywords

leucine-rich repeat kinase 2; Parkinson's disease; neurodegeneration; inflammation; oxidative stress

[#]**Corresponding author:** Jason Cannon, Ph.D., Assistant Professor of Health Sciences and Toxicology, Purdue University, HAMP-1271, 550 Stadium Mall Dr., West Lafayette, IN 47907, Tel: (765) 494-0794 Fax: (765) 496-1377, cannonjr@purdue.edu.

[*]These authors contributed equally to this manuscript.

Disclosure statement. The authors declare no actual or potential conflicts of interest.

1. Introduction

A major pathological hallmark of Parkinson's disease (PD) is progressive degeneration of dopaminergic (DA) neurons in the substantia nigra (SN), with a variety of other neuronal populations also being affected (Braak et al., 2003; Forno, 1996). Despite largely unknown etiology of most PD cases, G2019S mutation in leucine-rich repeated kinase 2 (LRRK2, G2019S substitution at the conserved Mg^{++}-binding motif in kinase domain) is the most common genetic cause of PD and G2019S LRRK2 mutation accounts for 5–6% of dominantly inherited familial and 1–2% of sporadic PD (Gandhi et al., 2009; Gilks et al., 2005; Zimprich et al., 2004). PD caused by LRRK2 mutations is typically clinically and pathologically indistinguishable from sporadic PD (Healy et al., 2008).

LRRK2 has multiple functional domains including Ras-like small GTPase domain and MAPKKK-like kinase domain (Guo et al., 2006). LRRK2 is expressed in diverse mammalian cell types. In the brain, LRRK2 is expressed in subcellular components, including cytoskeletal structures of diverse neuronal cell types (Biskup et al., 2006). In neurons, the physiological function of LRRK2 has been reported to mediate microglial proinflammatory response, regulation of cytoskeleton, or synaptic vesicle storage and mobilization, as well as MAPK kinase signaling (Gloeckner et al., 2009; MacLeod et al., 2006; Moehle et al., 2012; Piccoli et al., 2011). Much data suggests that kinase activity in LRRK2 likely mediates mutant LRRK2-induced neurotoxicity (Lee et al., 2010; Moehle et al., 2012; Smith et al., 1985; Yang et al., 2012). However, elucidating the normal physiological and pathological functions of LRRK2 remains difficult with unknown substrate of LRRK2. To understand the *in vivo* neuropathological function of G2019S LRRK2 protein in the LRRK2-mediated PD pathogenesis, a mammalian model expressing G2019S LRRK2 is needed.

Previous transgenic LRRK2 mouse models developed did not confirm overexpression of LRRK2 in the SN pars compacta and did not reproduce DA neuron loss (Li et al., 2010; Li et al., 2009; Melrose et al., 2010). Although, two G2019S LRRK2 transgenic mouse models constructed using intrastriatal viral vector injection reproduced neurodegeneration of nigral DA neurons, they have limitations in LRRK2 expression: 1) restricted expression in the nigrostriatal DA system – the expression pattern bears limited relevance to LRRK2 expression observed in the postmortem brain of LRRK2-linked PD patients (Giasson et al., 2006); 2) diminishing LRRK2 expression over time, which is unlikely to occur in humans (Dusonchet et al., 2011; Lee et al., 2010). In the present study, human G2019S LRRK2 transgenic (TG) rats constructed using bacterial artificial chromosome (BAC) technology were characterized in terms of behavior, neurochemistry, and neuropathology to unravel the pathogenic role of G2019S LRRK2. A recent brain distribution study in BAC-transgenic mice and rats (including the line used in this study) suggests that this technology is well suited to achieving overexpression in the nigrostriatal dopamine system (West et al., 2014). We hypothesized that G2019S LRRK2 BAC TG rats would show robust overexpression of LRRK2 in neurons of different brain regions, which would induce PD-related alterations in behavior, neurochemistry, and neuropathology.

2. Materials and Methods

2.1. Animals

G2019S LRRK2 transgenic (TG) Sprague-Dawley rats were produced using bacterial artificial chromosomal technology (BAC) similar to previously described (Cannon et al., 2013). These animals were developed by the laboratory of DR. Chenjian Li and through a program sponsored by the Michael J Fox Foundation are now commercially available (Taconic, Hudson, NY, U.S.A.). TG rats and non-TG littermate controls (WT) (44 WT & 46 TG rats, all male) were obtained from Taconic. All procedures were approved by the Purdue University Committee on the Care and Use of Animals.

2.2. Behavioral analysis

2.2.1. Postural instability—Postural instability was assessed as described (Woodlee et al., 2008). This test has also been shown to be useful to detect bilateral motor deficits(Cannon et al., 2009; Tapias et al., 2014). Briefly, the rat was held near vertical over sandpaper (grit: 150, 3MHR8, W.W. Grainger Inc., USA) attached onto hard glass plate, with a ruler attached on the side of plate. One fore-limb was lightly restrained against the animal's torso by the tester and the other fore-limb made contact with the plate. When viewed directly above, the rat's nose tip was aligned with start line of ruler and the animal was moved forward over the planted limb, and when the rat made a catch-up step to regain its weight balance, distance was calculated. Three trials were performed for each limb. When 6 measurements for both limbs were completed, the 6 values were pooled together, and the highest and lowest measurements were excluded. The remaining 4 measurements were averaged for each animal. At each time point, 7–10 animals were tested for each group.

2.2.2. Rearing—Rearing is an exploratory behavior of rat. The rearing test was conducted as described elsewhere (Fleming et al., 2004; Tillerson et al., 2001). Briefly, rearing was assessed by quantifying forelimb contact to a transparent cylinder wall (20 cm diameter/ 30 cm height). The number of contacts made by a rat was recorded using video camera for 5 min and counted by a blinded experimenter. To be classified as a rear, the rat had to raise forelimbs above shoulder and contact the cylinder wall with both or either limb(s). The rat had to land both forelimbs on the ground before making another quantifiable rear. This test has been shown to effectively identify locomotor deficits in bilateral PD models (Cannon et al., 2009; Tapias et al., 2014).

2.3. Western blotting

To confirm expression levels of transduced human G2019S LRRK2 BAC TG rat, western blot of LRRK2 was performed in tissue samples from the striatum, cortex, hippocampus, and ventral midbrain of TG and WT at 8 months age. Rats were euthanized by decapitation. The brain was surgically removed and coronal 2 mm sections of striatum, frontal cortex, hippocampus, and ventral midbrain were dissected on ice, flash frozen in liquid nitrogen, and then stored at −80 °C until use.

Western blot on LRRK2 was performed as described by Davies (Davies et al., 2013). Briefly, each tissue was homogenized in PBS containing 1× protease inhibitor (Halt™

protease inhibitor cocktail, Thermo Scientific, Rockford, IL, USA) using a dounce homogenizer (1 mL, Wheaton Science, Millville, NJ, USA). The homogenate was centrifuged at 20,000 × *g* for 5 min at 4 °C. The supernatant was assayed for protein content by the bicinchoninic acid method (Smith et al., 1985),(Pierce BCA Protein Assay Kit, Thermo Scientific) to load equal amount of protein in a polyacrylamide gel (PAGE, 7.5%, Mini Protean TGX precast polyacrylamide gel, Bio-Rad Lab, Inc., USA). After the protein assay, the calculated amount of supernatant was mixed with sampling buffer (95% Laemmli buffer, Bio-Rad; 5% β-mercaptoethanol, Sigma-Aldrich, St. Louis, MO, USA) and then incubated for 30 min at room temperature (RT). The lysate was electrophoresed at 120 V for 90 min in SDS-PAGE. Then, the gel was blotted onto a methylated PVDF membrane (Bio-Rad) in transfer buffer containing 10% methanol and 0.025% SDS with ice-pack at 100 V for 1 h and then 35 V, overnight. After 3 PBS washes, the membrane was blocked in PBS containing 5% bovine serum albumin (Jackson ImmunoResearch, West Grove, PA, USA) and 0.1% Tween-20 (Bio-Rad) for 90 min at RT. The membrane was incubated in primary antibodies in PBS containing 5% BSA and 0.1% Tween-20 at 4 °C overnight: mouse anti-LRRK2 N241A/34 (1:1000, 75–253, NeuroMab, Davis, CA, USA) and chicken anti-β-tubulin (1:1000, AB9354, Millipore, Temecula, CA, USA). Importantly, the chosen LRRK2 antibody has been evaluated in a rigorous multi-laboratory study for specificity in both immunoblotting and immunohistochemical experiments (Davies et al., 2013; West et al., 2014). After 3 PBS washes, the membrane was incubated in secondary antibodies (IR800 donkey anti-mouse, 1:5000, 926–32212 and IR680 donkey anti-chicken, 1:20,000, 926–68075, Li-Cor, Lincoln, NE, USA) for 2 h at RT, followed by 6 washes in PBS. The membrane was scanned using an Odyssey infrared scanner (resolution: 84 μm; Li-Cor, Lincoln, NE, USA) and single bands at size ~260 kDa were selected and quantified using the Image Studio software (ver. 3.1, Li-Cor). Fluorescence intensity for LRRK2 was expressed relative to β-tubulin to control for protein loading. LRRK2 expression in TG rats was normalized to the mean WT value, in each brain region.

2.4. Tissue processing and immunohistochemical determination of LRRK2

Rats were deeply anesthetized with pentobarbital (> 50 mg/kg) (Beuthanasia-D Special, Schering-Plough Animal Health Corp., Union, NJ, USA) and then transcardially perfused with 100–150 mL PBS followed by 250–300 mL 4% buffered paraformaldehyde (PFA), and the brains were surgically removed. The brains were post-fixed in 4% PFA for 24 h and then were saturated with 30% sucrose at 4 °C for at least 3 days. Within a week after sinking, each brain was coronally sectioned on a frozen sliding microtome (35 μm thick, Microm HM 450, Thermo Scientific, Rockford, IL, USA). Free-floating immunohistochemistry was performed as described by Davies *et al.*, 2013 (Davies et al., 2013). Briefly, after 6 PBS washes (10 min each) the section was quenched in 0.3% hydrogen peroxide in cold methanol. Antigen was retrieved in 10 mM sodium citrate (pH 6.0, Sigma-Aldrich) containing 0.05% Tween-20 (Bio-Rad, USA) at 37°C for 30 min. Two blockings were performed: first with 3% non-fat dry milk and the second with 10% normal donkey serum (NDS, Jackson ImmunoResearch, West Grove, PA, USA) both in PBS containing 0.3% triton x-100 (PBST). After PBS washes, the sections were incubated in primary antibody, mouse anti-LRRK2 (1:2000, N241/34, 75–253, NeuroMab, Davis, CA, USA) in PBST containing 5% NDS at 4 °C for 24 h. Following 3 PBS washes, the sections were incubated

in biotinylated donkey anti-mouse (1:200, 715-065-151, Jackson ImmunoResearch, West Grove, PA, USA) in PBST containing 5% NDS at 4°C for 24 h. Then, the sections were washed 3 times in PBS and incubated in pre-mixed avidin-biotin complex (Vector Labs, Burlingame, CA, USA) for 1h at RT. Following 3 PBS washes, the sections were developed in 3,3´-diaminobenzidine (DAB) substrate (Vector Labs) for 1.5–2 min and then washed immediately in PBS (6 times) and mounted on glass microscopy slides (Fisher Scientific, Waltham, MA, USA). After air-drying overnight, the sections were dehydrated in graded ethanol and Histoclear (National Diagnostics, Atlanta, GA, USA) and then coverslipped using Histomount (National Diagnostics).

To determine if LRRK2 expression was localized in nigral DA neurons, immunofluorescence staining was conducted. Staining was performed as above, with the omission of hydrogen peroxide treatment and using the following primary antibodies [sheep anti-tyrosine hydroxylase (1:2000, AB1542, Millipore, Billerica, MA, USA) and mouse anti-LRRK2 (1:1000, N241/34, 75–253, NeuroMab)] and secondary antibodies [Cy3 donkey anti-sheep (1:500, 713-165-147, Jackson ImmunResearch) and Alexa 488 donkey anti-mouse (1:500, 715-545-151, Jackson ImmunoResearch)].

2.5. Light microscopy

For immunoblotting on LRRK2, an Olympus BX53 light microscope with Olympus DP72 digital camera was used to take chromogenic images using the CellSens Dimension software. Images were acquired at 10× magnification (N.A. 0.3). For optimal comparison, all images were taken under the same settings and adjustments to brightness and contrast were made equally across all images.

2.6. Confocal Microscopy

Except where otherwise indicated, immunofluorescent stained images were obtained using a Nikon A1R confocal microscope (Nikon Instruments, Melville, NY, USA) and processed using NIS-elements (ver., 4.13). Adjustments were performed equally across all images.

2.7. Neurotransmitter quantification

Neurotransmitter analysis was conducted similarly to as previously described (Cannon et al., 2009; Tapias et al., 2014; Wang et al., 2014). Briefly, after rats were sacrificed by decapitation, whole brains were quickly removed, cooled in ice-cold PBS, dissected in a brain mold on ice, flash frozen and then stored at −80 °C until analyses. Frozen brain tissue samples were sonicated (40% power, 2:1 pulse, 45 seconds, Ultrasonic processor, Model FB120, Pittsburgh, PA, USA) in cold 0.4 N perchloric acid and centrifuged at 16,100 × g, 4 °C for 35 min. Then, after the supernatant was collected and filtered in Costar Spin-X (0.22 μm nylon membrane, Corning, NY, USA), the lysate was stored at −80 °C. The pellet was resuspended in 0.1 M NaOH for protein quantification. Levels of DA, DOPAC (3,4-dihydroxyphenylacetic acid), HVA (homovanillic acid), serotonin (5-HT), 5-Hydroxyindoleacetic acid (5-HIAA) and norepinephrine (NE) were analyzed using high-performance liquid chromatography with electrochemical detection (HPLCECD, Dionex Ultimate 3000 HPLC, Thermo Scientific, Rockford, IL, USA) and an autosampler within the separation module. The HPLC mobile phase contained: 0.08 M sodium phosphate

monobasic, 8% methanol, 2% acetonitrile, 2.0 mM 1-octanesulfonic acid, 0.025 mM ethylenediaminetetraacetic acid, and 0.2 mM triethylamine, at pH 2.4. Chromatography was isocratic with a flow rate of 0.6 mL/min. The mobile phase passed through a pre-column guard cell to oxidize contaminants, set at 450 mV. Neurotransmitters were separated on a 150 × 3.2mm C18 column (MD-150, Thermo Scientific) with a 3.0 μm particle size, passed through a conditioning cell at −150 mV and detected on a Coulochem III electrochemical detector with an analytical cell set at 350 mM (Thermo Scientific). The separation and detection occurred at 32 °C. Neurotransmitters were determined as ng analyte per mg protein and quantified using a standard curve generated from injection of standards (Sigma-Aldrich) of the highest available purity. Protein concentration in the tissue samples was determined by the bicinchoninic acid protein assay method (Smith *et al.*, 1985, Pierce BCA Protein Assay Kit, Thermo Scientific) in a 96-well plate, using bovine serum albumin standard (Thermo Scientific).

2.8. Striatal terminal density quantification

To determine whether G2019S LRRK2 expression in the TG rat induce degeneration of DA neuron terminal, immunohistochemistry on tyrosine hydroxylase (TH, the rate-limiting enzyme in DA synthesis) was conducted at the ages of 4, 8, and 12 months. Striatal terminal density was assessed on the same brains utilized for neurochemistry. The second brain hemisphere was removed as described in Neurochemistry section and was post-fixed in 4% PFA for 7 days and then saturated in 30% sucrose until sinking. Then, it was sectioned on dry ice (35 μm thick) using sliding microtome mentioned above and stored in cryoprotectant at −20 °C until use. The fluorescent immunostaining was performed as described earlier (Cannon et al., 2011; Tapias et al., 2014). Briefly, the section was incubated mouse anti-TH (1:2000, MAB318, Millipore, Temecula, CA, USA) in PBST 48–72 h at 4 °C. For secondary antibody, the sections were incubated in IR800 donkey anti-mouse (1:500, 926–32212, Li-Cor, Lincoln, NE, USA) for 2 h at RT. Then, tissue was rinsed 6 times in PBS, air-dried, and mounted using DPX mounting medium (Prolabo, VWR international, USA). The sections were scanned on an Odyssey infrared scanner (Li-Cor) and fluorescence intensity in dorsal striatum was quantified and averaged over 4–6 sections/rat as previously described (n = 7–10/group).

2.9. Morphological assessment of nigral dopamine neurons

To assess gross changes in cellular morphology, cresyl violet (Nissl) staining was conducted as previously described (Kiernan, 2008). Specific changes in cell morphology, such as elongation and shrinkage, are directly related to cell death. Phenotypic alterations in cellular size or shape have been observed during apoptosis, both *in vivo* and *in vitro* (Kermer et al., 2002; LaFerla et al., 1997). To examine if the G2019S LRRK2 mutation leads to neuronal degeneration, SN serial sections from 12 month-old TG rats were immunostained for TH and nuclei. Pictures were acquired using laser scanning confocal microscope at 60× and quantitative assessment of morphologic features was performed as previously described, using the MetaMorph software (Tapias and Greenamyre, 2014; Tapias et al., 2013). Briefly, each cell was assigned a shape factor by the software, a value from 0 to 1 representing the circularity of an object. A value near 0 reveals a flattened object, whereas a value near to 1 indicates a perfect circle. Five SN sections per rat were analyzed (n = 4 rats/group).

2.10. Quantification of oxidative stress in tissue and single cells

To determine whether G2019S LRRK2 overexpression induces oxidative stress the following endpoints were assessed: (i) oxidized/reduced thiol ratio; (ii) nitrotyrosine (3-NT) levels; and (iii) inducible nitric oxide synthase (iNOS) levels.

2.10.1. Histological thiol labeling in SN Pars Compacta—Histological thiol staining was performed as previously described (Horowitz et al., 2011). Rats were deeply anesthetized and sacrificed by decapitation. Brains were removed and immediately frozen in liquid nitrogen. For thiol staining, all brains being compared were processed the same day, with the same solutions. Brains were cut on a cryostat (20 μm sections), placed on slides and immediately fixed for 30 min with a solution of 4% paraformaldehyde, 10 μM *N*-ethylmaleimide (Acros, Geel, Belgium), and 1 μM Alexa 680 maleimide (Life Technologies, Grand Island, NY, USA) to label reduced thiol groups (S-H). After the first labeling step, excess alkylating reagents were removed with three five-min PBS washes, and sections were reduced with 5 mM tris (2-carboxyethyl) phosphine (TCEP) in PBS, for 30 min. After a quick wash in PBS, a solution with10 μM *N*ethylmaleimide and 1 μM Alexa 547 maleimide (Invitrogen) was used to label the previously oxidized oxidized thiol groups (S-S). Ratiometric confocal analysis of thiol and disulfides was performed with an Olympus Fluoview 1000 laser scanning confocal microscope. The pinhole was adjusted to obtain a 1 μm thick optical slice (single plane/image). Region of interest (ROIs) were manually generated around single neurons. The software measures the signal intensity within the ROIs. The detection parameters were set in the control reaction and were kept constant across specimens. The ratio S-S/S-H signal was calculated by the confocal software, which also generated the ratio images. The ratio was set equal to 100% in the control specimen, which was the control reaction of hippocampal neurons for all the experiments.

2.10.2. Histological thiol labeling in Striatum—Striatal sections for thiol labeling were obtained from the same animals as above. The sections were scanned on an Odyssey infrared scanner and fluorescence intensities S-H (680 nm) or S-S (800 nm) in striatum were quantified and analyzed as S-S/S-H ratio.

2.10.3. Nitrotyrosine levels in nigral dopamine neurons—Tyrosine nitration of proteins is a feature of aging and several pathologies associated with an excessive generation of reactive nitrogen (and oxygen) species. Immunofluorescence staining was conducted in DA neurons as above with the use of the 3-NT antibody (rabbit anti-NT, 1:500, #06-284, Millipore) (Cannon et al., 2013; Tapias et al., 2014). Analysis of the confocal images was conducted using the Fluoview imaging software to quantify 3-NT immunofluorescence at 60×.

2.11. Neuroinflammation analysis

To identify whether neuroinflammation occurs as a result of G2019S expression, biochemical and morphological endpoints were examined.

2.11.1. iNOS levels in nigral dopamine neurons—Excess nitric oxide levels have been implicated in a variety of neurodegenerative diseases, including PD (Doherty, 2011).

Under pathophysiological conditions, the inducible isoform of nitric oxide synthase (iNOS) is robustly upregulated, which plays a central role in imflammation (Halliwell and Gutteridge, 2007). To investigate the effect of G2019S mutation on LRRK2 nitric oxide production, quantitative fluorescence microscopy was used to determine the expression levels of iNOS (mouse anti-iNOS, 1:5000, ab49999, Abcam, Cambridge, MA, USA) in TH-immunoreactive neurons (Tapias et al., 2014). Assessment of iNOS was performed on confocal images that were acquired with the same laser intensity with magnification at 60×. An average of 200–300 DA neurons was examined and data from each nigral section and were combined in order to calculate means. Five SN sections per animal, 5 rats per group were analyzed.

2.11.2. Microglia density and Morphology—Evidence of microglial activation has been observed in postmortem brain of PD patients and PD animal models. Further, LRRK2 has been postulated to play a role both in systemic and neuroinflammation (Lin et al., 2009; Moehle et al., 2012). To determine whether G2019S LRRK2 expression in rat evokes microglial activation in the SN at 12 months of age, five SN sections from 5 animals/group were labeled using anti-TH and anti- Iba1 antibodies and appropriate fluorescently conjugated secondary antibodies. Iba-1 immunoreactive cells were analyzed using a novel approach (Tapias and Greenamyre, 2014; Tapias et al., 2013); images of nigral brain sections were obtained on an automated Nikon 90i microscope platform equipped with a digital camera. The scanning was carried out using a motorized XYZ stage capable of high-speed image acquisition and assembly of up to 400 images from four different light channels into a single montage. The NIS-Elements software was used of scanning the entire surface of the SN; then, images were exported to ImageJ software for determination of morphological activation, number of microgial-positive cells, and total area occupied by the microglial particles. Five SN sections per rat were analyzed (n = 5 rats/group). Data represents pixels from five nigral sections per animal; each treatment group was comprised of 5 rats.

2.11.3. Astrocyte morphology—Immunofluorescent staining for glial fibrillary acidic protein (GFAP) (primary antibody: rabbit anti-GFAP, 1:500, Z0334, Dako, Carpinteria, CA, USA; secondary antibody: Alexa 647 donkey anti-rabbit, 1:500, Jackson ImmunoResearch) and TH was conducted as described in section 2.4. Images were acquired using confocal microscopy as described in section 2.6. Here, Z-stacked images over 2 μm were obtained at 0.2 μm intervals.

2.12. Statistical analysis

All results were statistically analyzed using the Prism 6.0 (GraphPad Software, Inc., La Jolla, CA, USA). Unpaired Student's t-test was applied to compare TG and WT at each time point, except for shape factor. Data for shape factor ranged from 0 (flat) to 1 (circular) and did not exhibit Gaussian distribution (p <0.0001, D'Agostino and Pearson omnibus normality test). Thus, shape factor data was analyzed by the nonparametric Mann-Whitney U-test. All values are presented as the mean ± standard error of mean (S.E.M.) unless noted otherwise and comparisons with p <0.05 were deemed significantly different.

3. Results

3.1. Western blot (LRRK2 expression)

LRRK2 expression in TG was significantly higher than that in littermate controls (WT, Fig. 1A–C). Expression in TG rats was typically ~5–8 times greater compared to WT, depending on brain region (Fig. 1B, C): striatum (485 ± 22 vs. 100 ± 22; TG vs. WT; p <0.0001, n = 3) and hippocampus (781 ± 48 vs. 100 ± 10; p <0.0001, n = 3/group). Moreover, LRRK2 expression in TG rats was clearly evident in the cortex and ventral midbrain (Fig. 1A). Direct quantitative comparison between WT and TG in cortex and ventral midbrain was not possible due to LRRK2 being virtually undetectable in WT in these brain regions.

3.2. Immunohistochemistry of LRRK2 expression

To determine localized expression of LRRK2 protein in each of 4 different brain regions, immunohistochemistry on LRRK2 was performed. Chromogenic staining for LRRK2 showed overt increases in cellular staining in the 4 brain regions of TG rat compared to those of WT (Fig. 2A). In each brain region assessed, staining was primarily evident in the cells with neuronal morphology. Of note, is clear expression in the pars compacta region of the SN. Striatal expression appeared to be limited to select populations of cell bodies with a lack of clear expression in striatal terminals, similarly to a recent report (West et al., 2014). Immunofluorescence staining indicated within the midbrain that LRRK2 was highly localized in dopamine neurons (TH^+) in the SN (Fig. 2B).

3.3. Motor behavioral deficits

Postural instability and rearing tests were conducted to determine whether G2019S LRRK2 expression leads to behavioral motor changes at 4, 8, and 12 months age. G2019S LRRK2 overexpression in TG rats did not induce prominent changes in postural instability up to 12 months age. Thus, there is not clear evidence of clear motor phenotype. However, age-dependent alterations were observed. Postural instability was increased in TG compared to WT at 8 months age (Fig. 3A, 4.8 ± 0.2 vs. 4.0 ± 0.2: distance to trigger (cm); p <0.05, n = 7–9/group). In the rearing, test while G2019S LRRK2 expression in TG did not cause significant changes up to 8 months age, at 12 months age G2029S LRRK2 expression significantly increased number of rearing in TG compared to WT (Fig. 3B, 15 ± 1 vs. 10 ± 1; p <0.05; n = 9–10/group).

3.4. Neurotransmitter levels

3.4.1. Striatal dopamine and metabolites—Expression of G2019S LRRK2 in TG rats did not induce changes in striatal DA, DOPAC, DA turnover rate levels in 8 and 12 months old rats (Fig. 4). However, significant changes in HVA were observed at 12 months of age (11.1 ± 0.4 vs. 9.3 ± 0.5; TG vs. WT; ng/mg protein; p <0.05, n = 7–10). Thus, we conclude that up until 12 months of age, TG rats do not exhibit loss of striatal DA.

3.4.2. Striatal serotonin and metabolites—G2019S LRRK2 expression did not induce detectable changes in striatal 5-HT, 5-HIAA, or 5-HT turnover rate of TG rat compared to WT at 8 and 12 months age (Fig. 5).

3.5. Striatal dopaminergic terminal density

G2019S LRRK2 rats did not exhibit any significant changes in striatal TH immunofluorescence compared to WT at 4, 8, and 12 months age (Fig. 6A, B). Thus, we conclude that expression of G2019S LRRK2 in these rats does not produce an overt lesion to striatal dopamine terminals.

3.6. Morphological changes in DA neurons of the SN

Overt loss of nigrostriatal DA neurons was not observed in TG rats, and gross changes in cellular morphology were not observed in the SN after Nissl staining (Fig. 7A, B). However, detailed, quantitative morphometric analysis proved that DA neurons in the SN pars compacta of TG rats exhibited an abnormally elongated cell body compared to WT (Fig. 7C–H). Overall cell body area of DA neuron in TG rat was not altered (Fig. 7G), whereas the shape factor (morphological measurement of flatness of a shape) of DA neurons in TG rats was significantly flattened compared to WT at 12 months age (Fig. 7H) [0.0150 ± 0.003 vs. 0.0276 ± 0.004; p <0.001; TG vs. WT; Mann-Whitney U test; n = 1016–1220 DA neurons analyzed/group (4 animals/group)].

3.7. Oxidative stress

3.7.1. Oxidized/reduced thiol ratio in SN pars compacta and striatum—G2019S LRRK2 expression induced oxidative stress (oxidized S-S/reduced SH thiol ratio) in the nigrostriatal DA system (Fig. 8A, C). The ratio of oxidized S-S/reduced SH thiols was normalized to mean control values. In individual DA neurons of the SN, the ratio was increased nearly 2-fold in TG rats (Fig. 8B, 190.3 ± 0.5 vs. 107.7 ± 0.9; TG vs. WT; p <0.001, n = 332 DA neurons/group) and in the dorsolateral striatum of TG rats, tissue level oxidation ratios were increased ~1.5-fold compared to WT rats (Fig. 8D, 138.1 ± 4.8 vs. 100.0 ± 2.3; TG vs. WT; p <0.0001, n = 18 striatum/group).

3.7.2. Nitrotyrosine levels in nigral dopamine neurons—3-NT levels (relative to mean control) in nigral dopamine neurons (Fig. 9) were increased nearly 2-fold in rats (Fig. 9I) expressing G2019S LRRK2 compared to WT (192.5 ± 14.3 vs. 100.0 ± 7.6; TG vs. WT; p <0.001; n = 5/group) in the absence of a loss of TH expression (Fig. 9J).

3.8. Neuroinflammation

3.8.1. iNOS levels in nigral dopamine neurons. iNOS levels (relative to mean control) in nigral dopamine neurons (Fig. 10) were increased nearly 2-fold in rats (Fig. 10I) expressing G2019S LRRK2 compared to WT (172.3 ± 15.2 vs. 100.0 ± 12.04; TG vs. WT; p <0.01; n = 5/group) in the absence of a change in TH expression (Fig. 10J).

3.8.2. Microglia density and morphology—There were no overtly detectable differences in SN microglial density and/or morphology between TG and WT rats (Fig. 11A–D). Quantitative stereological and morphometric analysis conducted on Iba-1 positive cells did not elucidate differences between WT and TG in microglial activation, number, or overall cell area (pixels), respectively (Fig. 11E–G).

3.8.3. Astrocyte activation—Immunofluorescence staining for GFAP$^+$ cells in the SN did not indicate any overt evidence of astrocyte activation in TG rats (Fig. 11H–M).

4. Discussion

Mutations in LRRK2 are the most frequent cause of genetic PD. However, suitable animal models expressing these mutations do not yet exist. Here, we have characterized a newly available BAC-transgenic model. Our results indicate that up until at least 12 months of age, G2019S LRRK2 overexpression in TG rats did not induce overt nigrostriatal DA neurodegeneration, characteristic of late-stage PD. However, we did find evidence that this model may replicate key preclinical features of PD, specifically, significant evidence of oxidative stress in SN DA neurons and their projections and morphological aberration of SN DA neurons were found.

Key pathological hallmarks of PD include nigral DA neuron and striatal terminal loss, resulting in striatal DA depletion, resulting in characteristic motor deficits (Cannon and Greenamyre, 2010). In this study, we did not find evidence that this model replicates the key features of end-stage PD. This conclusion was evidenced by: (i) lack of consistent behavioral deficits (Fig. 3); (ii) undetectable changes in striatal DA levels or DA terminal density (Figs. 4, 6); and (iii) absence of microglial activation (Fig. 11).

Our results suggest that certain preclinical alterations potentially relevant to PD are evident. Importantly, our results revealed that G2019S LRRK2 TG rats presented: (i) modest evidence of behavioral alterations (Fig. 3); (ii) changes in HVA levels (Fig. 4); (iii) SN DA neuron morphological alterations (Fig. 7); (iv) evidence of oxidative stress, both in striatal tissue and individual nigral DA neurons (Figs. 8, 9); and (v) significant iNOS activation, which can generate large amounts of nitric oxide that can be genotoxic and pro-inflammatory (Fig. 10). Taken together, these findings indicate that this new animal model may be useful to study preclinical endpoints.

Although *in vitro* studies have reported neuronal cell death in human R1441C and G2019S LRRK2 TG cells compared to WT (Smith et al., 2006; Smith et al., 2005) most *in vivo* studies using transgenic models have not produced detectable cell loss (Herzig et al., 2012; Li et al., 2009; Melrose et al., 2010; Tong et al., 2009). Rather, Li and colleagues (Li et al., 2009) found TH-positive axons beaded and fragmented with spheroids and dystrophic neurites, indicative of abnormal morphology. Interestingly, G2019S LRRK2 rodent models using intrastriatal viral vector infusion induced nigral DA neuron degeneration in contrast to WT LRRK2 rodent (Dusonchet et al., 2011; Li et al., 2010). In the same study, the authors could not detect any protein at the size expected for monomeric LRRK2 in SN, nor in striatal extracts (Dusonchet et al., 2011). Further, LRRK2 expression was shown to diminish over time. In contrast, BAC TG mice studies have reported 5–10 times increased LRRK2 expression in comparison to endogenous levels (Li et al., 2010; Li et al., 2009), which is in a similar range to our findings. Further, a recent detailed neuroanatomical report on this and other BAC LRRK2 lines in both mice and rats shows that overexpression is achieved in nigral DA neurons and that aberrant distribution in other neuronal cell-types also occurs in this line, with expression also evident in striatal cholinergic neurons (West et al., 2014).

Thus, our results are consistent also with the observation that LRRK2 localizes primarily in cells with neuronal morphology (Biskup et al., 2006; Dusonchet et al., 2011). Importantly, the expression within the nigrostriatal DA system is primarily limited to SN DA cell bodies (Fig. 2), with limited evidence of striatal terminal expression. Validated LRRK2 antibodies have only recently become available and the LRRK2 epitope is highly sensitive to degradation (Davies et al., 2013). Thus, careful examination of LRRK2 expression in human brain still needs to be conducted.

Taken together, it is possible that acute local LRRK2 expression increases induced by vector infusion produces very different physiological responses compared to lifetime expression occurring in BAC-TG animals, which replicates a temporal expression pattern similar to humans (Giasson et al., 2006). A previous study – using mouse WT and G2019S LRRK2 BAC TG mice – reported that WT LRRK2 overexpression induced hyperactivity and increased performance in motor function tests, but G2019S LRRK2 overexpression did not induce changes (Li et al., 2010). Similarly, expression of human G2019S LRRK2 in BAC TG mice, without overall locomotor activity changes, showed abnormal exploratory activity behavior in open field analysis, including increased anxiety behavior, compared to WT or non-TG (Melrose et al., 2010). A transient increase in motor skill learning in human G2019S LRRK2 and WT LRRK2 was found in 3–4 month old mice, but not in older mice; analogous findings were observed for other motor tests (Herzig et al., 2012). Possible explanations in phenotypic differences in motor activity and DA terminal transmission among previous studies include differences in specific mutation (R1441G, R1441C, G2019S), expression levels of LRRK2, species (mouse/rat), and strains. As described in this work, no overt lesion to the nigrostriatal DA system was observed in previous studies.

Here, we have shown limited evidence of postural instability and potential hyperactivity (Fig. 3). Thus, results from our studies are consistent with other attempts to create animal models expressing disease-causing LRRK2 mutations. Modest behavioral changes might come from subtle alterations in axon terminal DA transmission. Previous studies reported impaired DA transmission (extracellular release), without alteration of tissue DA content in R1441G, R1441C, and G2019S LRRK2 TG animals (Li et al., 2009; Melrose et al., 2010; Tong et al., 2009). An age-dependent decrease in striatal DA levels, DA uptake and release in LRRK2 G2019S mice compared to LRRK2-WT, or non-TG littermate controls without motor deficits or nigrostriatal DA lesion have been also reported (Li et al., 2010). In our study, elevated HVA was observed in TG rats. HVA is considered the final metabolite in DA catabolism (Gnegy, 2012). Thus, mounting data suggests that expression of mutated LRRK2 affect DA neurotransmission, in the absence of eliciting a direct lesion to the system.

Oxidative stress has been repeatedly reported in experimental PD models and and post-mortem brain of PD patients. DA neurons are particularly susceptible to oxidative stress (Dauer and Przedborski, 2003; Fahn and Cohen, 1992). A recent study reported that DA neurons in TG flies expressing human G2019S LRRK2 were more vulnerable to oxidative stress than flies expressing WT human LRRK2 (Yang et al., 2012). Here, we report evidence that G2019S expression produces oxidative stress in the striatum and within DA neurons of the SN as evidenced by both increases in thiol oxidation and nitrosylated proteins. To the best of our knowledge, this is the first report to show LRRK2-mediated increased oxidative

stress in the nigrostriatal DA system in a rodent model. While in future studies it may be useful to examine oxidative stress in other neuronal populations, for the reasons mentioned above, it is expected that DA neurons would be selectively sensitive to LRRK2-mediated increases in oxidative stress. Increased oxidative burden may explain the heightened sensitivity to oxidative insults observed in a variety of other *in vitro* and *in vivo* models expressing mutated LRRK2.

Neuroinflammation plays a significant role in the pathogenesis of PD. LRRK2's potential role in systemic inflammatory bowel disease has piqued interest that the protein has a role in systemic inflammation (Liu et al., 2011; Liu and Lenardo, 2012). In our study, significant increased iNOS immunoreactivity was observed in SN DA neurons of animals expressing G2019S, which may be suggestive of biochemical evidence of neuroinflammation (likely through modulation of the expression of multiple pro-inflammatory genes). Increased iNOS expression in brain has been shown in multiple neurotoxicant PD animal models (Guo et al., 2006; Liberatore et al., 1999; Tapias et al., 2014; Thakur and Nehru, 2013). In addition, microglial activation has been found in these experimental animal models and in human PD (Tufecki et al., 2012). However, our data showed that G2019S LRRK2 expression alone did not induce microglial activation which is consistent with previous studies (Herzig et al., 2012; Lin et al., 2009). Mutant or WT expression in the striatum of mice significantly was, however, found to exacerbate microgliosis in the presence of mutant α-synuclein overexpression (Lin et al., 2009). LRRK2 inhibition alleviated inflammatory responses in a lipopolysaccharide-induced rodent model of neuroinflammation (Moehle et al., 2012). It is worth noting that examination of inflammation-related endpoints typically is conducted during late-stage PD in patients, or after significant SN DA cell death has occurred in animal models.

In the current study, we assessed animals up until 12 months of age. It is possible that behavioral, neurochemical, or pathological alterations may not become apparent until near the end of life span, much later than 12 months of age. Our data on dopaminergic neuron morphology, in particular supports the rationale for such studies. Here, we observed cellular elongation. Such morphological changes have been observed during apoptosis, both *in vivo* and *in vitro* (Kermer et al., 2002; LaFerla et al., 1997). Thus, the morphological changes observed in our TG rats may be indicative of impeding cell death. Full life-span studies would however require significant resources and diet restriction to prevent morbid obesity that typically occurs in aged, *ad libitum* fed rats. Ideally, an additional TG line expressing WT human LRRK2 would have served as an excellent control but, unfortunately, such a line does not currently exist. Importantly, the majority of the literature cited above suggests that biochemical effects of exogenous LRRK2 expression are mutation-dependent.

In summary, although we did not observe overt DA neuron loss in the SN, striatal DA depletion, or behavioral changes, we found evidence of oxidative stress, iNOS overexpression, and abnormal morphology of nigral DA neurons. Our data suggests that an initial consequence of G2019S LRRK2 overexpression is a subtle biochemical changes rather than overt denervation of nigrostriatal DA neurons. Thus, the G2019S LRRK2 BAC TG rats may be used as a valuable preclinical model of early biochemical impairments. Further, potentiation studies utilizing environmental exposures may be particularly useful in

examining gene-environment interactions, given the incomplete penetrance of LRRK2 mutations.

Acknowledgements

Funding. This work was supported by the Michael J. Fox Foundation (grants to J.R.C. and J.T.G.), the National Institute of Environmental Health Sciences at the National Institutes of Health [R00S019879 and R03ES022819 to J.R.C.], and the Ralph W. and Grace M. Showalter Research Trust [to J.R.C. and J-.C.R.].

Additional acknowledgements. We would like to thank Dr. Chenjian Li for the creating this new TG line and also depositing it into Taconic as a public resource. Also, we would like to thank Stefanie O'Neal for technical help in behavior tests.

References

Biskup S, Moore DJ, Celsi F, et al. Localization of LRRK2 to membranous and vesicular structures in mammalian brain. Ann Neurol. 2006; 60:557–569. [PubMed: 17120249]

Braak H, Del Tredici K, Rub U, et al. Staging of brain pathology related to sporadic Parkinson's disease. Neurobiol Aging. 2003; 24:197–211. [PubMed: 12498954]

Cannon JR, Geghman KD, Tapias V, et al. Expression of human E46K-mutated alpha-synuclein in BAC-transgenic rats replicates early-stage Parkinson's disease features and enhances vulnerability to mitochondrial impairment. Exp Neurol. 2013; 240:44–56. [PubMed: 23153578]

Cannon JR, Greenamyre JT. Neurotoxic in vivo models of Parkinson's disease recent advances. Prog Brain Res. 2010; 184:17–33. [PubMed: 20887868]

Cannon JR, Sew T, Montero L, et al. Pseudotype-dependent lentiviral transduction of astrocytes or neurons in the rat substantia nigra. Exp Neurol. 2011; 228:41–52. [PubMed: 21056560]

Cannon JR, Tapias V, Na HM, et al. A highly reproducible rotenone model of Parkinson's disease. Neurobiol Dis. 2009; 34:279–290. [PubMed: 19385059]

Dauer W, Przedborski S. Parkinson's disease: mechanisms and models. Neuron. 2003; 39:889–909. [PubMed: 12971891]

Davies P, Hinkle KM, Sukar NN, et al. Comprehensive characterization and optimization of anti-LRRK2 (leucine-rich repeat kinase 2) monoclonal antibodies. Biochem J. 2013; 453:101–113. [PubMed: 23560750]

Doherty GH. Nitric oxide in neurodegeneration: potential benefits of non-steroidal anti-inflammatories. Neurosci Bull. 2011; 27:366–382. [PubMed: 22108814]

Dusonchet J, Kochubey O, Stafa K, et al. A rat model of progressive nigral neurodegeneration induced by the Parkinson's disease-associated G2019S mutation in LRRK2. J Neurosci. 2011; 31:907–912. [PubMed: 21248115]

Fahn S, Cohen G. The oxidant stress hypothesis in Parkinson's disease: evidence supporting it. Ann Neurol. 1992; 32:804–812. [PubMed: 1471873]

Fleming SM, Zhu C, Fernagut PO, et al. Behavioral and immunohistochemical effects of chronic intravenous and subcutaneous infusions of varying doses of rotenone. Exp Neurol. 2004; 187:418–429. [PubMed: 15144868]

Forno LS. Neuropathology of Parkinson's disease. J Neuropathol Exp Neurol. 1996; 55:259–272. [PubMed: 8786384]

Gandhi PN, Chen SG, Wilson-Delfosse AL. Leucine-rich repeat kinase 2 (LRRK2): a key player in the pathogenesis of Parkinson's disease. J Neurosci Res. 2009; 87:1283–1295. [PubMed: 19025767]

Giasson BI, Covy JP, Bonini NM, et al. Biochemical and pathological characterization of Lrrk2. Ann Neurol. 2006; 59:315–322. [PubMed: 16437584]

Gilks WP, Abou-Sleiman PM, Gandhi S, et al. A common LRRK2 mutation in idiopathic Parkinson's disease. Lancet. 2005; 365:415–416. [PubMed: 15680457]

Gloeckner CJ, Schumacher A, Boldt K, et al. The Parkinson disease-associated protein kinase LRRK2 exhibits MAPKKK activity and phosphorylates MKK3/6 and MKK4/7, in vitro. J Neurochem. 2009; 109:959–968. [PubMed: 19302196]

Gnegy, ME. Catecholamines. In: Brady, ST.Siegel, GJ.Albers, RW., Price, DL., editors. Basic Neurochemistry. Principles of molecular, cellular, and medical neurobiology. 8th edition. New York, United States: Oxford University Press; 2012. p. 283-299.

Guo L, Wang W, Chen SG. Leucine-rich repeat kinase 2: relevance to Parkinson's disease. Int J Biochem Cell Biol. 2006; 38:1469–1475. [PubMed: 16600664]

Halliwell, B., Gutteridge, JMC. Reactive species can be poisonous. In: Halliwell, B., Gutteridge, JMC., editors. Free Radicals in Biology and Medicine. 4th edition. New York, United States: Oxford University Press; 2007. p. 440-487.

Healy DG, Falchi M, O'Sullivan SS, et al. Phenotype, genotype, and worldwide genetic penetrance of LRRK2-associated Parkinson's disease: a case-control study. Lancet Neurol. 2008; 7:583–590. [PubMed: 18539534]

Herzig MC, Bidinosti M, Schweizer T, et al. High LRRK2 levels fail to induce or exacerbate neuronal alpha-synucleinopathy in mouse brain. PLoS One. 2012; 7:e36581. [PubMed: 22615783]

Horowitz MP, Milanese C, Di Maio R, et al. Single-cell redox imaging demonstrates a distinctive response of dopaminergic neurons to oxidative insults. Antioxid Redox Signal. 2011; 15:855–871. [PubMed: 21395478]

Kermer P, Krajewska M, Zapata JM, et al. Bag1 is a regulator and marker of neuronal differentiation. Cell Death Differ. 2002; 9:405–413. [PubMed: 11965493]

Kiernan, JA. Histological and Histochemical Methods. 4th edition. Oxfordshire, United Kingdom: Scion Publishing Ltd; 2008. Histological Staining in One or Two Colours, Chapter 6.

LaFerla FM, Troncoso JC, Strickland DK, et al. Neuronal cell death in Alzheimer's disease correlates with apoE uptake and intracellular Abeta stabilization. J Clin Invest. 1997; 100:310–320. [PubMed: 9218507]

Lee BD, Shin JH, VanKampen J, et al. Inhibitors of leucine-rich repeat kinase-2 protect against models of Parkinson's disease. Nat Med. 2010; 16:998–1000. [PubMed: 20729864]

Li X, Patel JC, Wang J, et al. Enhanced striatal dopamine transmission and motor performance with LRRK2 overexpression in mice is eliminated by familial Parkinson's disease mutation G2019S. J Neurosci. 2010; 30:1788–1797. [PubMed: 20130188]

Li Y, Liu W, Oo TF, et al. Mutant LRRK2(R1441G) BAC transgenic mice recapitulate cardinal features of Parkinson's disease. Nat Neurosci. 2009; 12:826–828. [PubMed: 19503083]

Liberatore GT, Jackson-Lewis V, Vukosavic S, et al. Inducible nitric oxide synthase stimulates dopaminergic neurodegeneration in the MPTP model of Parkinson disease. Nat Med. 1999; 5:1403–1409. [PubMed: 10581083]

Lin X, Parisiadou L, Gu XL, et al. Leucine-rich repeat kinase 2 regulates the progression of neuropathology induced by Parkinson's-disease-related mutant alpha-synuclein. Neuron. 2009; 64:807–827. [PubMed: 20064389]

Liu Z, Lee J, Krummey S, et al. The kinase LRRK2 is a regulator of the transcription factor NFAT that modulates the severity of inflammatory bowel disease. Nat Immunol. 2011; 12:1063–1070. [PubMed: 21983832]

Liu Z, Lenardo MJ. The role of LRRK2 in inflammatory bowel disease. Cell Res. 2012; 22:1092–1094. [PubMed: 22430149]

MacLeod D, Dowman J, Hammond R, et al. The familial Parkinsonism gene LRRK2 regulates neurite process morphology. Neuron. 2006; 52:587–593. [PubMed: 17114044]

Melrose HL, Dachsel JC, Behrouz B, et al. Impaired dopaminergic neurotransmission and microtubule-associated protein tau alterations in human LRRK2 transgenic mice. Neurobiol Dis. 2010; 40:503–517. [PubMed: 20659558]

Moehle MS, Webber PJ, Tse T, et al. LRRK2 inhibition attenuates microglial inflammatory responses. J Neurosci. 2012; 32:1602–1611. [PubMed: 22302802]

Piccoli G, Condliffe SB, Bauer M, et al. LRRK2 controls synaptic vesicle storage and mobilization within the recycling pool. J Neurosci. 2011; 31:2225–2237. [PubMed: 21307259]

Smith PK, Krohn RI, Hermanson GT, et al. Measurement of protein using bicinchoninic acid. Anal Biochem. 1985; 150:76–85. [PubMed: 3843705]

Smith WW, Pei Z, Jiang H, et al. Kinase activity of mutant LRRK2 mediates neuronal toxicity. Nat Neurosci. 2006; 9:1231–1233. [PubMed: 16980962]

Smith WW, Pei Z, Jiang H, et al. Leucine-rich repeat kinase 2 (LRRK2) interacts with parkin, and mutant LRRK2 induces neuronal degeneration. Proc Natl Acad Sci U S A. 2005; 102:18676–18681. [PubMed: 16352719]

Tapias V, Cannon JR, Greenamyre JT. Pomegranate juice exacerbates oxidative stress and nigrostriatal degeneration in Parkinson's disease. Neurobiol Aging. 2014; 35:1162–1176. [PubMed: 24315037]

Tapias V, Greenamyre JT. A rapid and sensitive automated image-based approach for in vitro and in vivo characterization of cell morphology and quantification of cell number and neurite architecture. Curr Protoc Cytom. 2014; 68:12 33 1–12 33 22. [PubMed: 24692056]

Tapias V, Greenamyre JT, Watkins SC. Automated imaging system for fast quantitation of neurons, cell morphology and neurite morphometry in vivo and in vitro. Neurobiol Dis. 2013; 54:158–168. [PubMed: 23220621]

Thakur P, Nehru B. Anti-inflammatory properties rather than anti-oxidant capability is the major mechanism of neuroprotection by sodium salicylate in a chronic rotenone model of Parkinson's disease. Neuroscience. 2013; 231:420–431. [PubMed: 23159314]

Tillerson JL, Cohen AD, Philhower J, et al. Forced limb-use effects on the behavioral and neurochemical effects of 6-hydroxydopamine. J Neurosci. 2001; 21:4427–4435. [PubMed: 11404429]

Tong Y, Pisani A, Martella G, et al. R1441C mutation in LRRK2 impairs dopaminergic neurotransmission in mice. Proc Natl Acad Sci U S A. 2009; 106:14622–14627. [PubMed: 19667187]

Tufekci KU, Meuwissen R, Genc S, Genc K. Inflammation in Parkinson's disease. Advances in protein chemistry and structural biology. 2012; 88:69–132. [PubMed: 22814707]

Wang Y, Lee JW, Oh G, et al. Enhanced synthesis and release of dopamine in transgenic mice with gain-of-function alpha6* nAChRs. J Neurochem. 2014; 129:315–327. [PubMed: 24266758]

Woodlee MT, Kane JR, Chang J, et al. Enhanced function in the good forelimb of hemi-parkinson rats: compensatory adaptation for contralateral postural instability? Exp Neurol. 2008; 211:511–517. [PubMed: 18417125]

West AB, Cowell RM, Daher JP, Moehle MS, Hinkle KM, Melrose HL, Standaert DG, Volpicelli-Daley LA. Differential LRRK2 expression in the cortex, striatum, and substantia nigra in transgenic and nontransgenic rodents. The Journal of comparative neurology. 2014; 522(11):2465–2480. [PubMed: 24633735]

Yang D, Li T, Liu Z, et al. LRRK2 kinase activity mediates toxic interactions between genetic mutation and oxidative stress in a Drosophila model: suppression by curcumin. Neurobiol Dis. 2012; 47:385–392. [PubMed: 22668778]

Zimprich A, Biskup S, Leitner P, et al. Mutations in LRRK2 cause autosomal-dominant parkinsonism with pleomorphic pathology. Neuron. 2004; 44:601–607. [PubMed: 15541309]

Highlights

- We characterized a BAC-transgenic rat line expressing human G2019S LRRK2
- Tissue G2019S LRRK2 expression was ~5–8 times higher than wild-type rat LRRK2
- G2019S LRRK2 expression reproduced features of early-stage Parkinson's disease (PD)
- Neurodegeneration characteristic of late-stage PD was not produced
- This model may be useful to study early-stage PD and gene-environment interactions

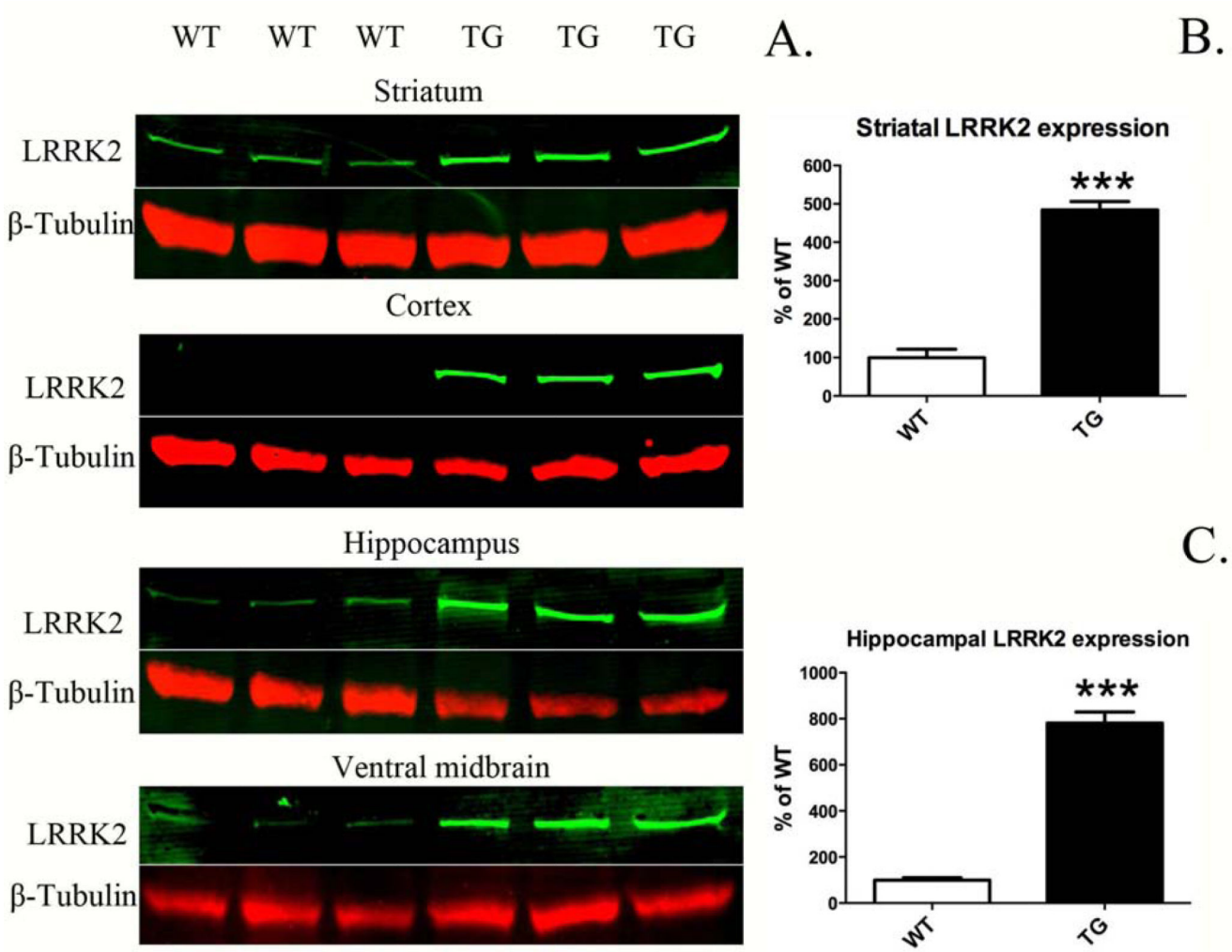

Figure 1.

LRRK2 expression in BAC-transgenic G2019S rats (TG) and wild-type (WT). ***A.*** Western blot analysis of LRRK2 in striatum, cortex, hippocampus, and ventral midbrain. ***B, C.*** Expression above baseline was quantified in brain regions, where LRRK2 expression was readily detectable in WT. Expression was quantified relative to β-tubulin (LRRK2/β-tubulin) and normalized to the mean WT value. ***p <0.001 versus WT, Student's t-test (n = 3/group; mean ± S.E.M.; LRRK2 expression analyzed at 8 months old).

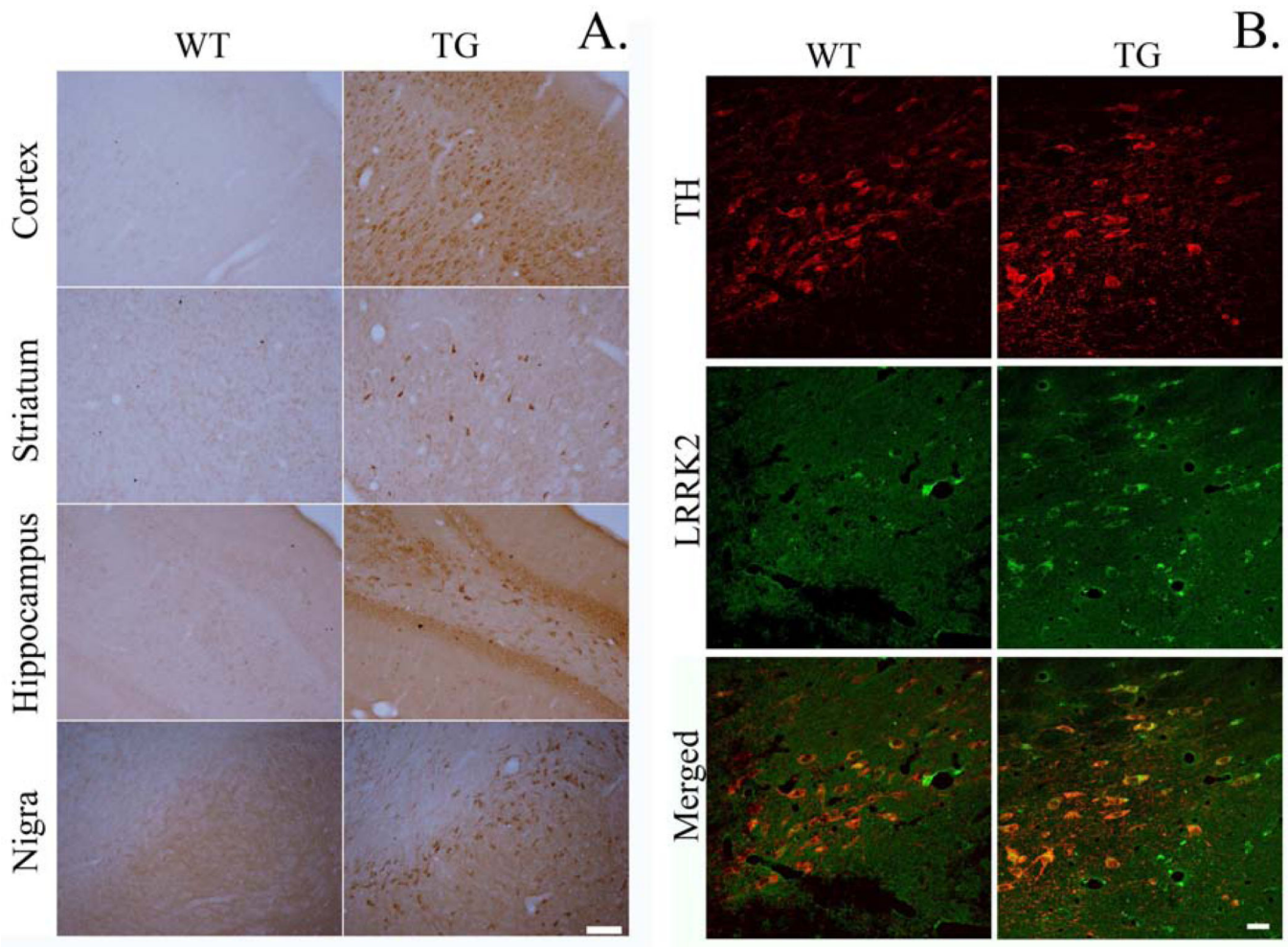

Figure 2.

A. Immunohistochemical staining for LRRK2 shows increased cellular expression in G2019S LRRK2 (TG) compared to wild-type (WT). Coronal brain slices containing cortex, striatum, hippocampus, and substantia nigra were stained for LRRK2. Scale bar = 100 μm.

B. Immunofluorescence staining indicated that LRRK2 was highly localized in dopamine (DA) neurons in the SN. Scale bar = 25 μm.

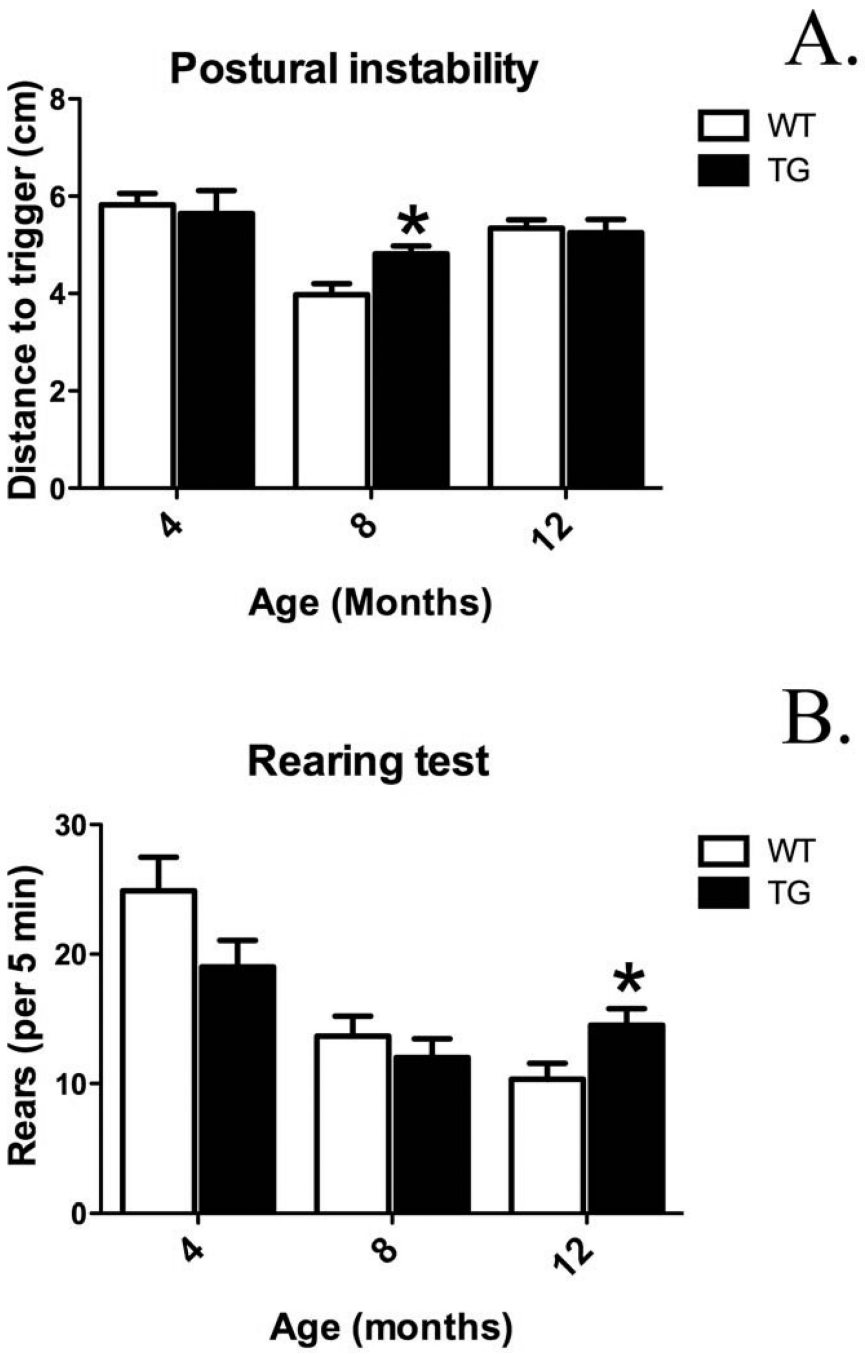

Figure 3.

Motor behavior alterations in BAC-transgenic G2109S LRRK2 rats (TG) at 4, 8, and 12 months old versus wild-type (WT) rats. ***A.*** Postural instability test [expressed as distance to trigger (cm)]. ***B.*** Rearing test (number of rears/5 min). *p <0.05 versus WT at specified time-point, Student's t-test (n = 7–10/group; mean ± S.E.M.).

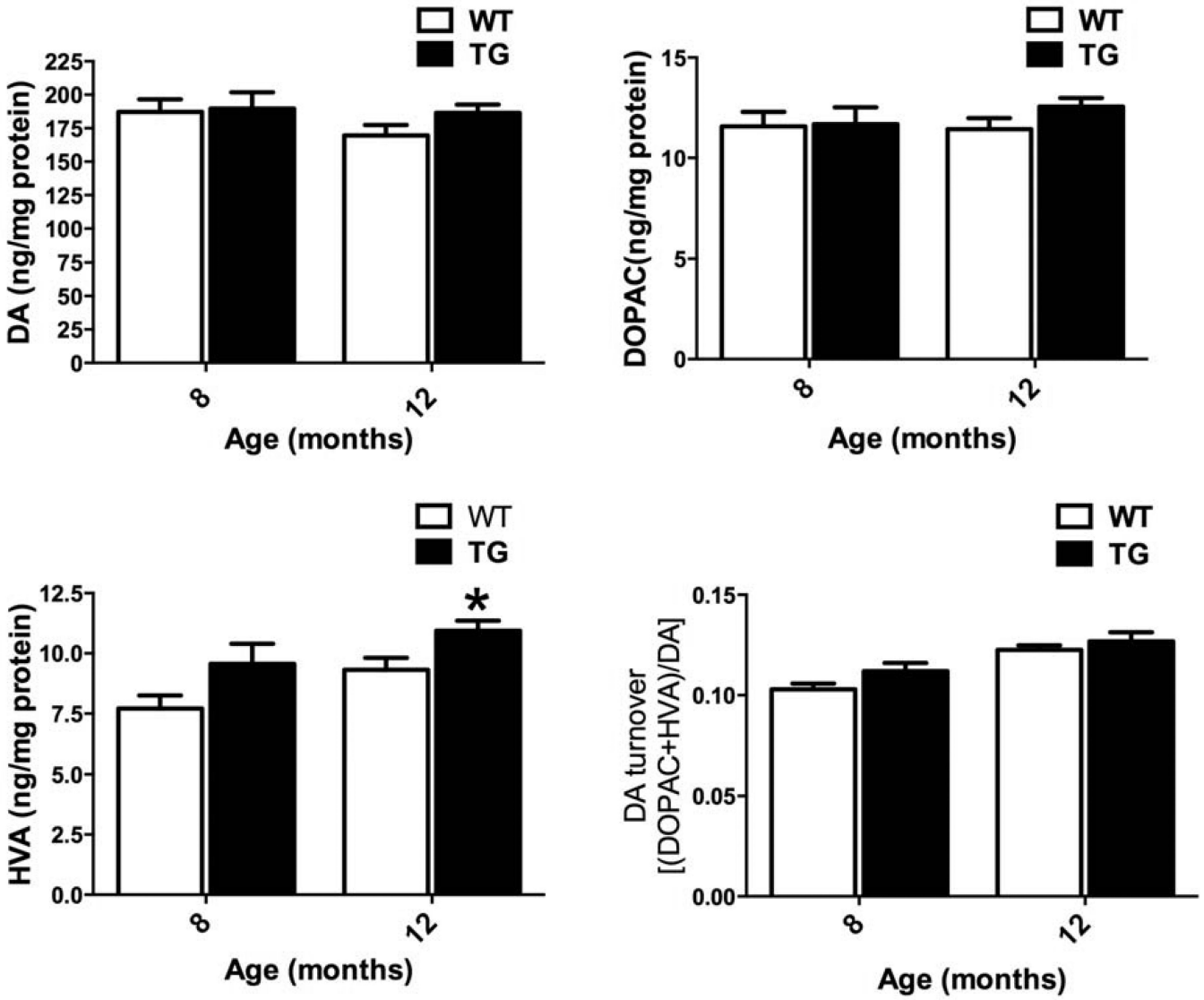

Figure 4.

Striatal dopamine (DA) and DA metabolites. G2019S LRRK2 (TG) expression does not induce alterations in striatal DA and induces minimal changes in DAergic metabolites [3,4-dihydroxyphenylacetic acid (DOPAC), homovanillic acid (HVA)]. Striatal DA and DAergic metabolites in TG and WT at 8, and 12 months old. DA turnover calculated as [(DOPAC + HVA)/DA]. *p <0.05 versus WT at specified time-point, Student's t-test (n = 7–10/group; mean ± S.E.M.).

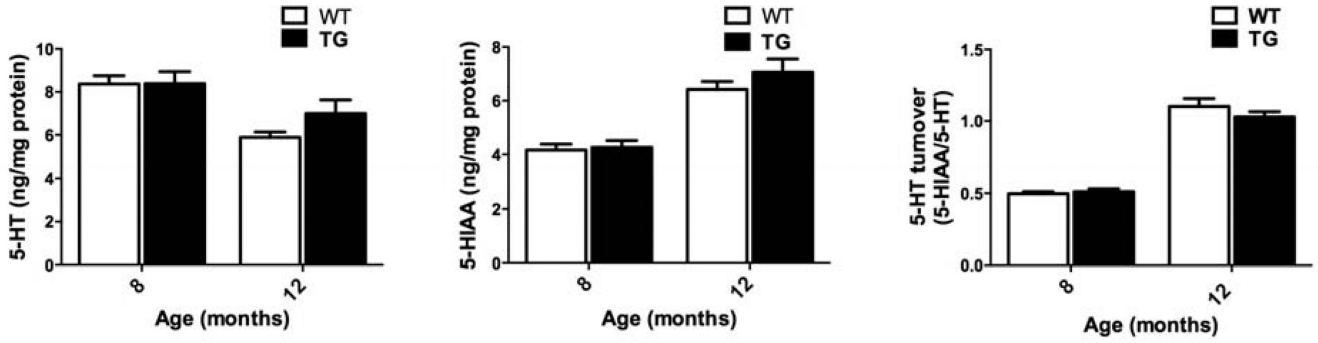

Figure 5.

Striatal serotonin (5-HT) and 5-hydroxyindoleacetic acid. G2019S LRRK2 (TG) expression does not alter the levels 5-HT or 5-hydroxyindoleacetic acid (5-HIAA) compared to WT at 8, and 12 months old. 5-HT turnover calculated as (5-HIAA/5-HT). Data expressed as mean ± S.E.M. n = 7–10/group.

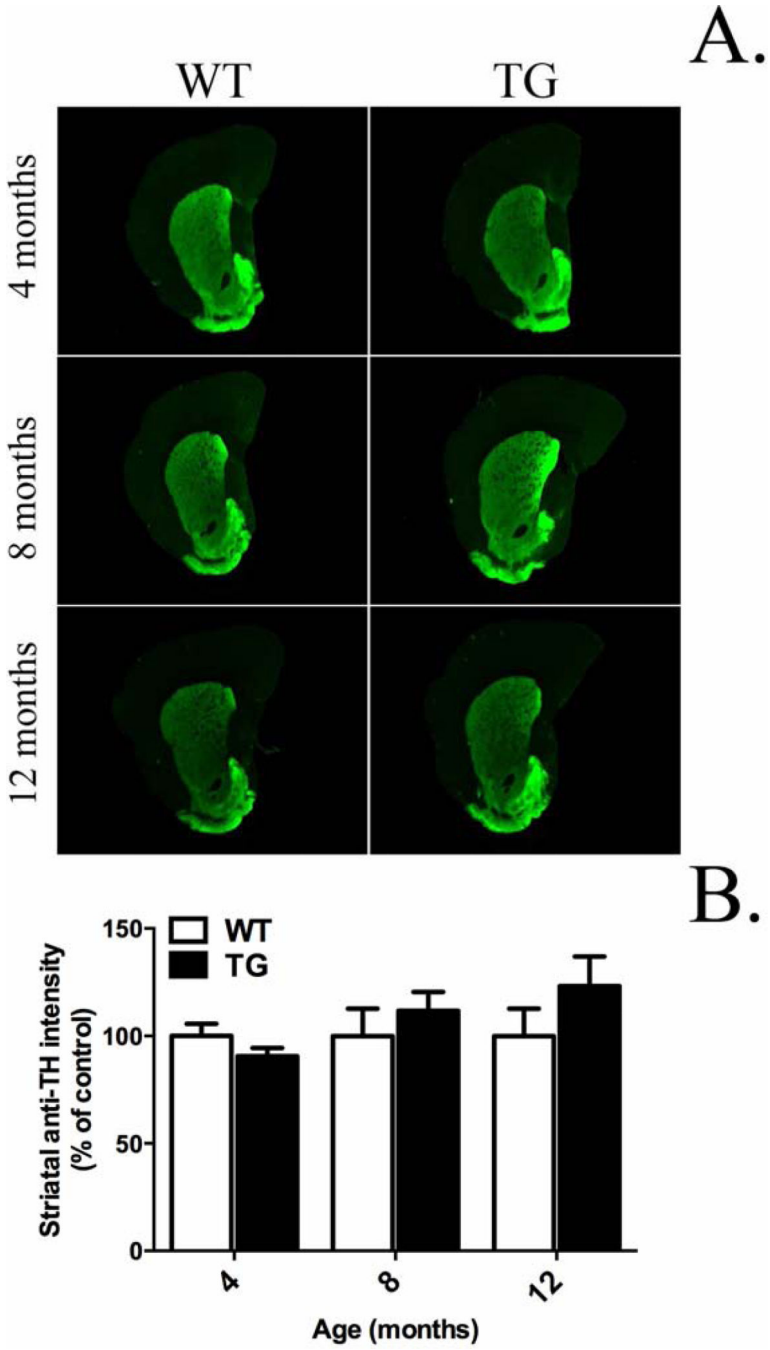

Figure 6.

Striatal dopamine terminal density. G2019S LRRK2 (TG) expression does not induce changes in striatal dopaminergic terminal density compared to wild-type (WT) at 4, 8, and 12 months old. Quantification was carried out in the dorsal striatum. The average immunofluorescence intensity for 3–5 coronal striatal slices was normalized to mean WT at specified time-point. Data expressed as mean ± S.E.M. n = 7–10/group.

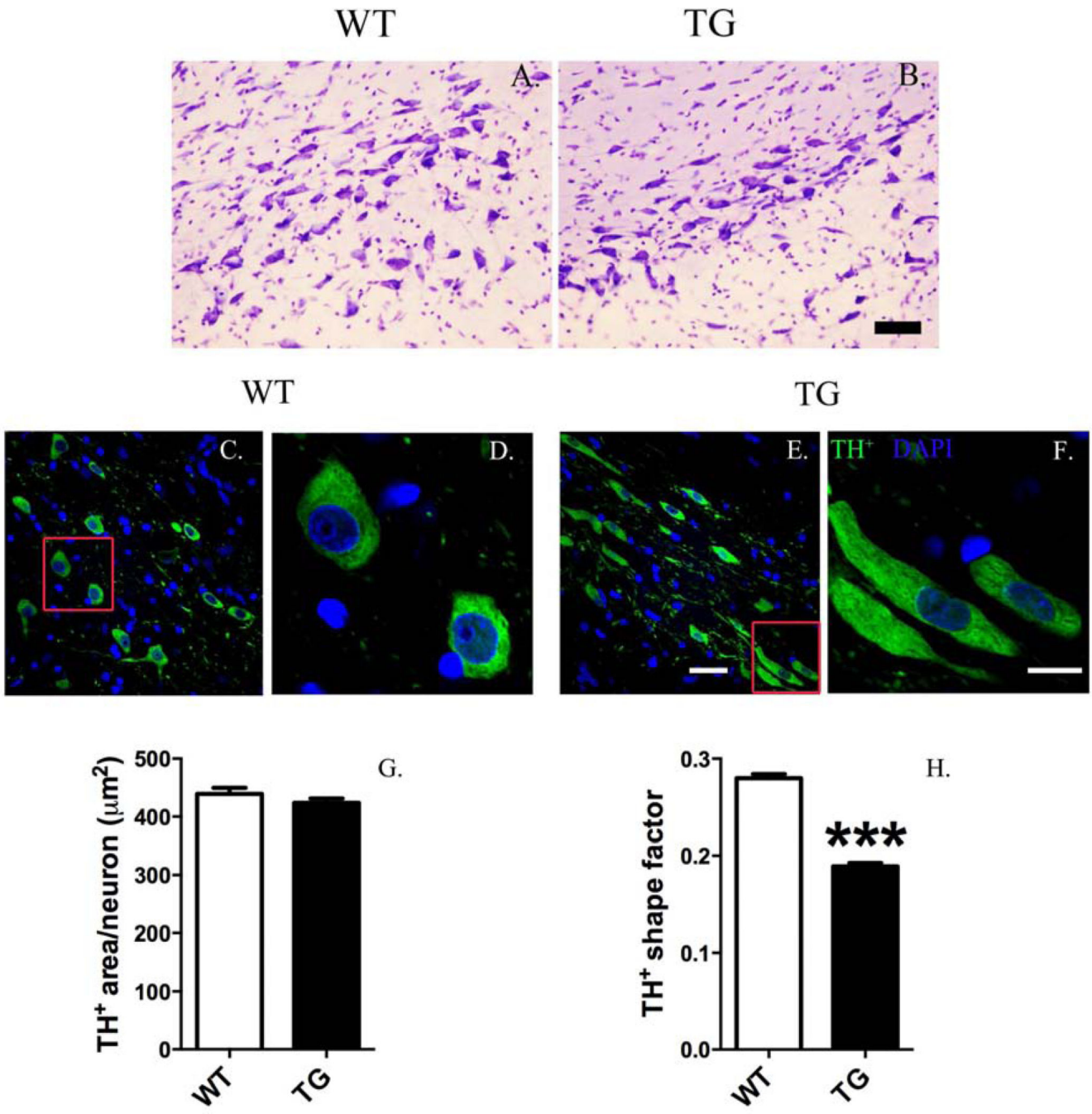

Figure 7.

Dopaminergic (DA) neurons in the substantia nigra of G2019S LRRK2 (TG) rats exhibit an abnormal, elongated morphology. Cresyl violet (Nissl) staining did not reveal gross changes in cellular morphology (scale bar = 50 μm) (***A, B***). However, quantitative, morphometric analysis of DA neurons revealed changes in cell shape. Low magnification images (***A, C***) show morphology differences in DA neurons (tyrosine hydroxylase^{+}, TH^{+}) between TG and wild-type (WT) (scale bar = 30 μm). High magnification images (***B, D***) show that DA neurons in TG rats exhibit an elongated cell body. Morphometric quantification shows that

overall cell body area is unchanged (***E***). Shape area significantly decreased in DA neurons of TG rats (a value from 0 to 1 representing the circularity of an object: a value near 0 reveals a flattened object, whereas a value near to 1 indicates a perfect circle). ***p <0.001, Mann-Whitney U-test versus WT [n = 1016–1220 DA neurons analyzed/group (4 animals/group); DA morphology analyzed at12 months old; data expressed as mean ± S.E.M.].

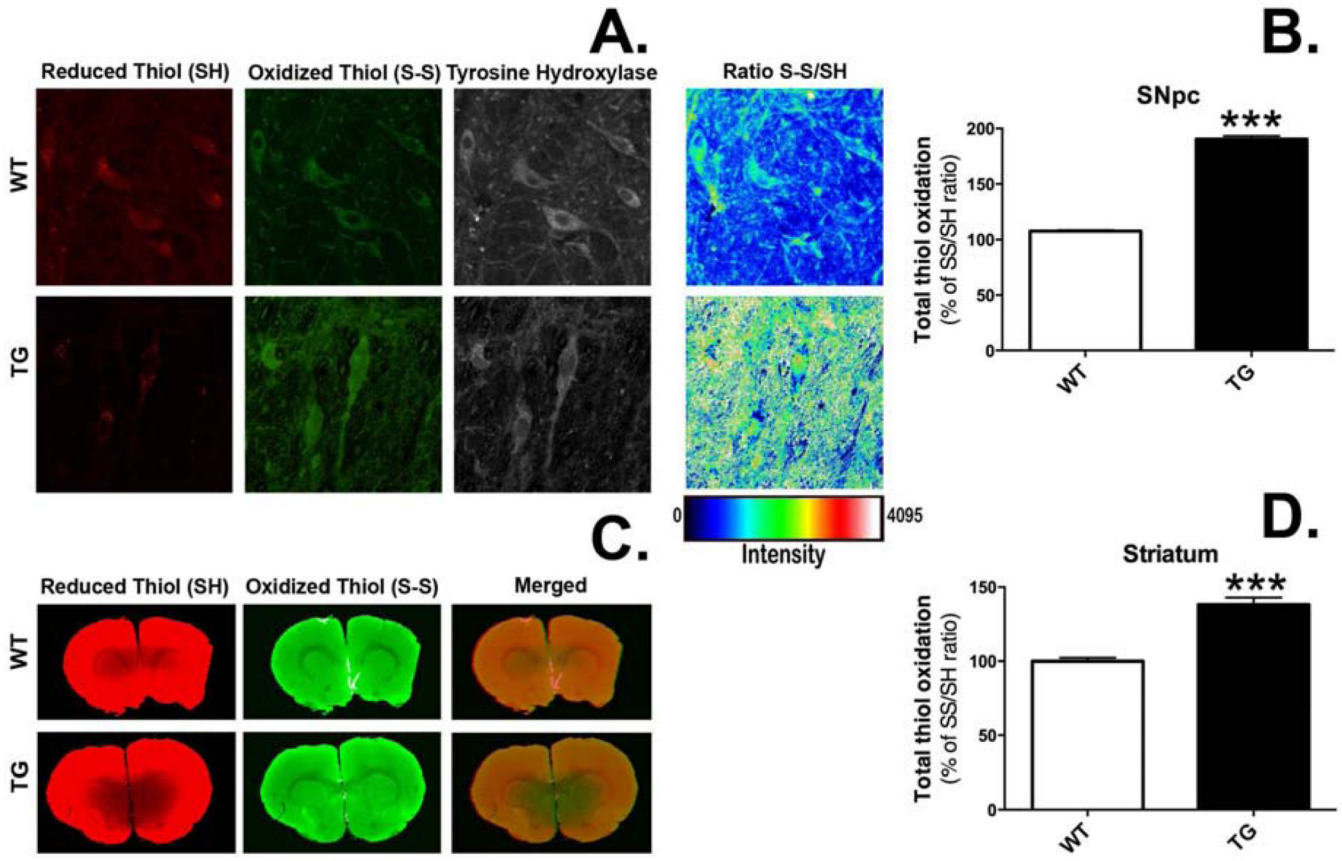

Figure 8.

Rats expressing G2019S LRRK2 (TG) exhibit evidence of increased thiol oxidation in the nigrostriatal dopamine (DA) system. Staining was performed in coronal brain sections for reduced and oxidized thiols in the pars compacta region of the substantia nigra (SN) (***A***) and the striatum (***B***). Regions of interest (ROIs) were drawn around single cells in the SN (n = 332 DA neurons/group) or the dorsolateral portion of the striatum (n = 18 striatal ROIs/group). Total thiol oxidation (SS/SH) was determined for each ROI. ***p <0.001 vs. wild-type (WT), Student's t-test (data expressed as mean ± S.E.M.).

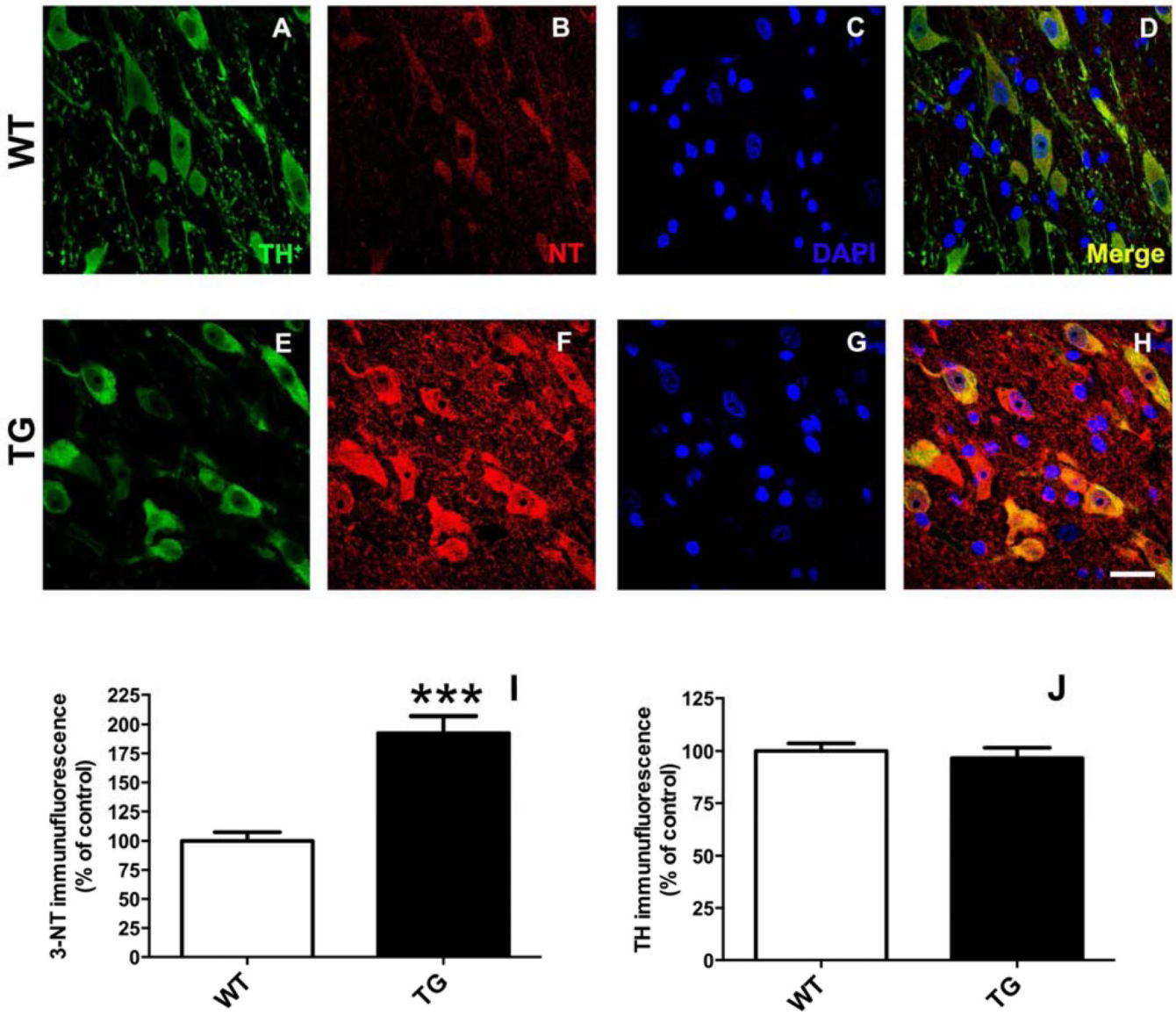

Figure 9.

Rats expressing G2019S LRRK2 (TG) exhibit evidence of increased protein nitrosylation in dopamine (DA) neurons of the substantia nigra (SN). Staining was performed in coronal brain sections for tyrosine hydroxylase (TH) (***A, E***) and 3-nitrotyrosine (NT) (***B, F***). Regions of interest (ROIs) were drawn around DAergic neurons (TH^+) in the pars compacta region of the SN. Quantitative immunofluorescence is reported (***I, J***) relative to mean control values (WT). ***p <0.001 vs. WT; n = 5/group; Student's t-test (data expressed as mean ± S.E.M.). TH levels were not significantly different between groups. Magnification bar = 20 μm.

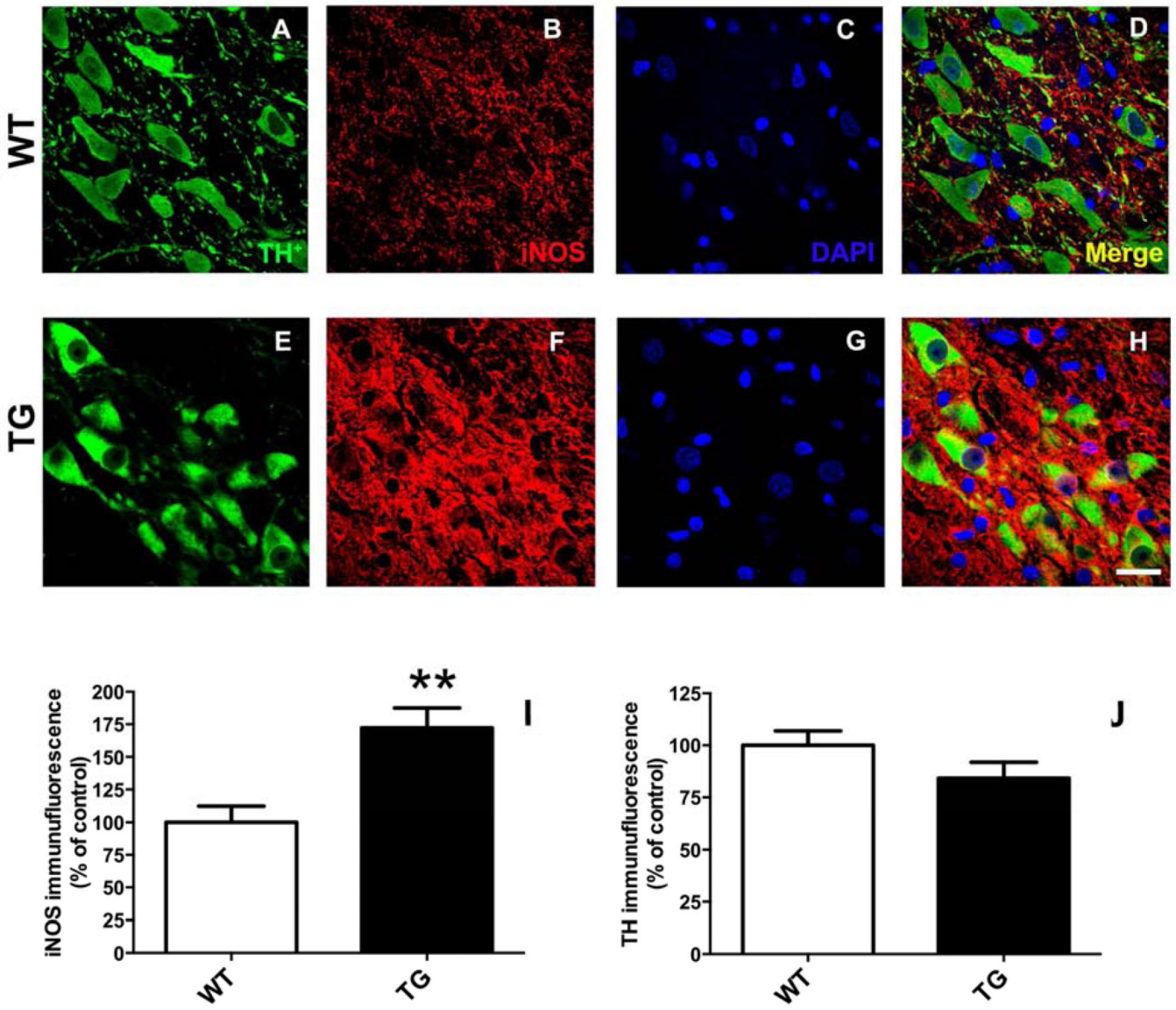

Figure 10.

Rats expressing G2019S LRRK2 (TG) exhibit evidence of increased expression inducible nitric oxide synthase (iNOS) in nigral dopamine (DA) neurons. Fluorescence immunostaining was performedin coronal brain sections for TH-immunopositive neurons (***A, E***) and iNOS (***B, F***). Regions of interest (ROIs) were drawn around DAergic neurons (TH^+) in the pars compacta region of the SN. Quantitative immunofluorescence is reported (***I, J***) relative to mean control values (WT). ***p <0.001 vs. WT; n = 5/group; Student's t-test (data expressed as mean ± S.E.M.). TH fluorescence intensity was similar between the experimental groups. Magnification bar = 20 μm.

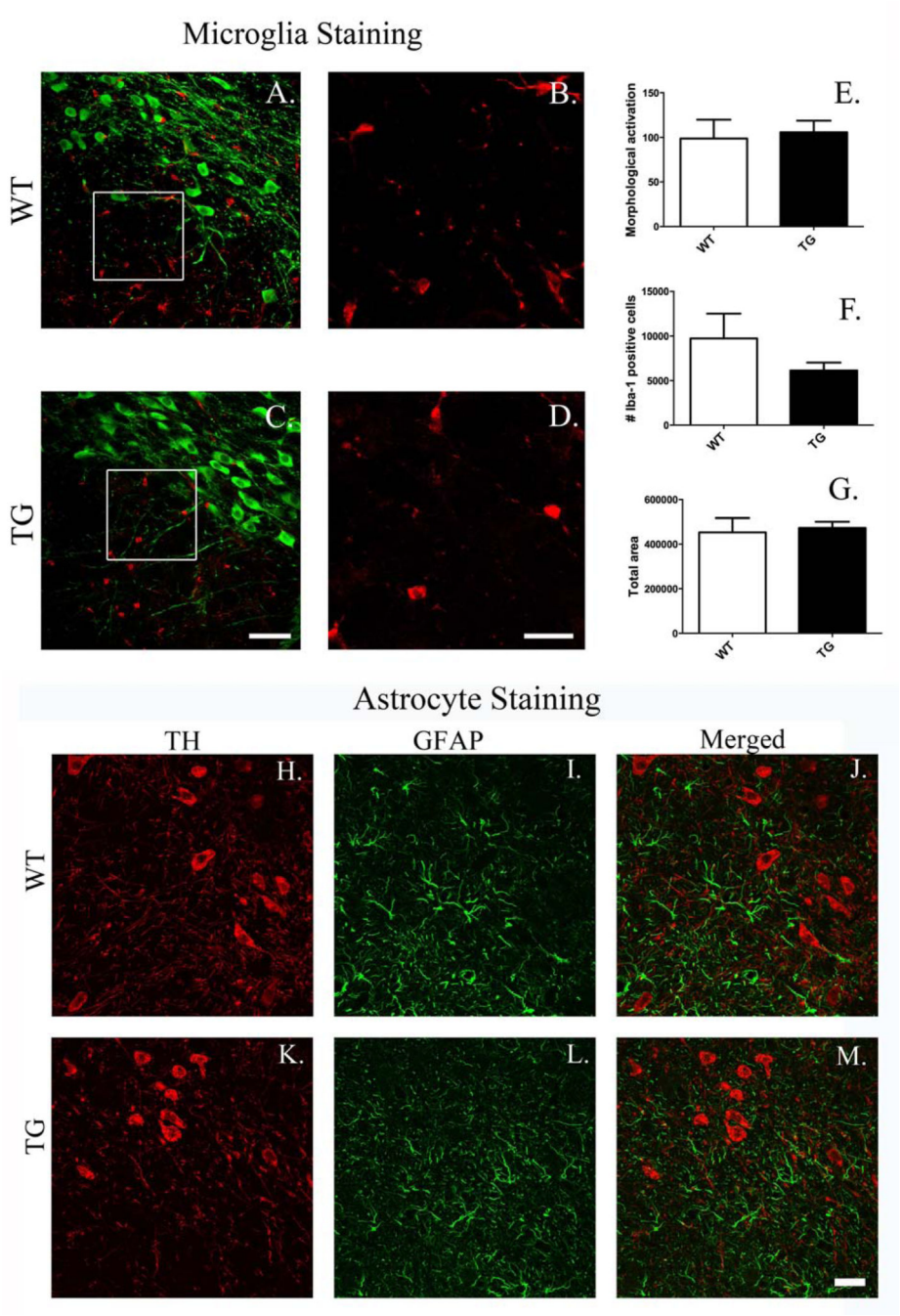

Figure 11.

Microglial and astrocyte morphology in the substantia nigra. There are no detectable differences in microglial density or morphology or in overt astrocyte activation between G2019S LRRK2 (TG) and wild-type (WT) rats in the substantia nigra. ***A, C*** show representative images of coronal sections stained for tyrosine hydroxylase (green) and Iba1 (red) (magnification bar = 50 μm). ***B, D*** Show high magnification images (insets from ***A, C***) of Iba^{+} cells (red) (magnification bar = 20 μm). No changes were detected in microglial density or morphology between G2019S LRRK2 TG (***C, D***) and WT (***A, B***) rats.

Quantitative stereological analysis conducted on Iba-1^+ cells did not reveal differences between groups in microglial activation (***E***), number (***F***), or overall cell area (pixels) (***G***) (4–5 sections/animal; n = 5/group; data expressed as mean ± S.E.M.). Glial fibrillary acidic protein (GFAP) staining (***I, L***) in the SN did not produce evidence of astrocyte activation in TG rats (***K–M***) compared to WT rats (***H–J***). Magnification bar = 25 μm.